



OPEN ACCESS

EDITED BY

Yang-Tse Cheng,
University of Kentucky, United States

REVIEWED BY

Janghyuk Moon,
Chung-Ang University, Republic of Korea
Ozan Toprakci,
Yalova University, Türkiye

*CORRESPONDENCE

Jiayang Li,
✉ j1306@uowmail.edu.au
Wei Kong Pang,
✉ wkpang@uow.edu.au
Bernt Johannessen,
✉ berntj@ansto.gov.au

RECEIVED 29 October 2025

REVISED 17 November 2025

ACCEPTED 25 November 2025

PUBLISHED 10 December 2025

CITATION

Wang X, Li J, Li X, Lee H, Tong Z, Pang WK and Johannessen B (2025) Engineering a composite solid-state electrolyte with multiple ionic channels for high-performance sodium metal batteries.
Front. Batter. Electrochem. 4:1734762.
doi: 10.3389/fbael.2025.1734762

COPYRIGHT

© 2025 Wang, Li, Li, Lee, Tong, Pang and Johannessen. This is an open-access article distributed under the terms of the [Creative Commons Attribution License \(CC BY\)](https://creativecommons.org/licenses/by/4.0/). The use, distribution or reproduction in other forums is permitted, provided the original author(s) and the copyright owner(s) are credited and that the original publication in this journal is cited, in accordance with accepted academic practice. No use, distribution or reproduction is permitted which does not comply with these terms.

Engineering a composite solid-state electrolyte with multiple ionic channels for high-performance sodium metal batteries

Xin Wang¹, Jiayang Li^{1*}, Xinghan Li¹, Hyojoo Lee^{1,2}, Ziwei Tong¹, Wei Kong Pang^{1*} and Bernt Johannessen^{1,3*}

¹Institute for Superconducting and Electronic Materials (ISEM), Australian Institute for Innovative Materials (AIMM), Innovation Campus, University of Wollongong, Wollongong, NSW, Australia, ²School of Advanced Materials Science and Engineering, Sungkyunkwan University, Suwon-si, Republic of Korea, ³Australian Synchrotron, ANSTO, Clayton, VIC, Australia

Composite solid-state electrolytes (CSSEs) represent a promising pathway toward advanced sodium metal batteries (SMBs), which are crucial for meeting the demand for higher energy density in electric vehicles and devices. However, the overall performance of SMBs, particularly in terms of safety and stability, remains below expectations due to limited ionic conductivity and interfacial uneven Na deposition. Herein, we develop an innovative composite solid-state electrolyte system that selects NASICON-type $\text{Na}_{3.7}\text{Zr}_{1.45}\text{Sc}_{0.4}\text{Mg}_{0.15}\text{Si}_2\text{PO}_{12}$ (NSMZSP) as an inorganic filler for incorporation into a polyvinylidene fluoride (PVDF) organic matrix. The optimized PVDF@NSMZSP CSSE creates multiple ionic transport channels along the PVDF, NSMZSP, and PVDF/NSMZSP interfaces, thus effectively promoting Na^+ transport dynamics and optimizing the electrolyte/electrodes interface compatibility. An exceptional ionic conductivity of $5.5 \times 10^{-4} \text{ S cm}^{-1}$ at room temperature and a high Na^+ transference number of 0.56 can be achieved accordingly. Full $\text{Na}/\text{Na}_3\text{V}_2(\text{PO}_4)_3$ cells employing this electrolyte deliver excellent rate capability and long-term cycling stability, maintaining a high initial discharge capacity of 95.7 mAh g^{-1} at 0.5 C, with a capacity retention of 95% after 200 cycles. This work demonstrates a promising CSSE system with fast ionic transportation, improved interfacial stability and sustainable cycle life, inspiring the construction of next-generation SMBs with well-designed CSSEs in the field of energy storage technology.

KEYWORDS

composite solid-state electrolytes, sodium metal batteries, fast ionic channels, interfacial compatibility, enhanced cycling stability

1 Introduction

The ongoing global transition toward transport decarbonization continues to drive the development of next-generation energy storage systems with higher energy density, lower cost, and enhanced safety (Du et al., 2025; Wang et al., 2022a). Among various energy storage technologies, conventional lithium metal batteries (LMBs) are widely preferred owing to their high specific capacity, wide operating voltage range, long cycle life and high

power density, earning them a reputation as the leading commercial technology (Armand and Tarascon, 2008; Li et al., 2018). Unfortunately, LMBs pairing lithium metal electrode with liquid electrolytes (LEs) face persistent challenges due to the scarcity and price volatility of lithium resources, as well as safety concerns arising from the flammable nature of LEs (Huang et al., 2025; Huang et al., 2023; Suh et al., 2025). The research focus has progressively transitioned to the modification of key battery components, where sodium metal batteries (SMBs) with functional solid-state electrolytes (SSEs) have emerged at the forefront of energy storage development owing to their advantages, such as the minimized risk of liquid leakage, ease of processability, improved lifetime, relatively higher power and energy densities (Hu et al., 2024; Famprikis et al., 2019). Nevertheless, the inherent barriers like sluggish room temperature ionic conductivity of SSEs and incompatible contact with electrodes are still exist, hindering their large-scale commercialization of SMBs in the short term (Lou et al., 2021; Dutra et al., 2025). Therefore, it is significant to develop advanced SSEs that ensure fast Na^+ transport and compatibility with both Na metal anode and positive cathodes (Fan et al., 2025; Huang et al., 2024).

Generally, SSEs for SMBs can be divided into three categories: inorganic solid-state electrolytes (ISSEs), polymer solid-state electrolytes (PSSEs) and composite solid-state electrolytes (CSSEs). ISSEs like Na- β -alumina, Na superionic conductors (NASICON) and sulfides, can exhibit relatively adequate room temperature ionic conductivity than that of conventional LEs, a high oxidative limit, and great thermal stability (Bay et al., 2020; Dong et al., 2025). Unfortunately, their rigid and rough surfaces brings unsatisfied solid-solid contact between ISSEs and electrodes, leading to high interfacial resistance. PSSEs made by dispersing various Na salts in polymer host materials like polyethylene oxide (PEO), polyvinylidene fluoride (PVDF), poly(vinylidene fluoride hexafluoropropylene) (PVDF-HFP), demonstrate soft mechanical properties that offer intimate contact with electrodes and feasible processability (Wang et al., 2025a; Wang et al., 2025b). While their low room temperature ionic conductivity, insufficient amorphous regions with a high degree of crystallinity significantly hinder their practical applications. Therefore, the incorporation of inorganic fillers into the PSSEs to create CSSEs has been verified to be an efficient strategy to possess compensated advantages of both ISSEs and PSSEs, thereby realizing enhanced ion conduction and interfacial compatibility. Among them, NASICON-type $\text{Na}_3\text{Zr}_2\text{Si}_2\text{PO}_{12}$ (NZSP) has been considered as a promising inorganic filler owing to its relatively high ionic conductivity at room temperature, wide electrochemical window, great air and chemical stability (Wang et al., 2025c). It is noteworthy that some delicate designed NZSP-based CSSEs for sodium batteries have been investigated in recent years (Wang et al., 2022; Wang et al., 2023b). For example, Wang et al. designed a hetero-layered composite polymeric electrolyte through uniformly adding NZSP nanofillers into PEO matrix (Wang et al., 2023c). A modified ionic conductivity of $1.62 \times 10^{-4} \text{ S cm}^{-1}$ at 60 °C and room-temperature cycling stability of 93.8% capacity retention for 200 cycles can be achieved accordingly. Similarly, Zhang et al. developed a solvent-free PEO-based CSSE filled with $\text{Na}_{3.4}\text{Zr}_{1.8}\text{Mg}_{0.2}\text{Si}_2\text{PO}_{12}$ ceramic, a great ionic conductivity of

$2.4 \times 10^{-3} \text{ S cm}^{-1}$ at 80 °C and $4.4 \times 10^{-5} \text{ S cm}^{-1}$ at room temperature can be obtained when 40 wt% inorganic filler was included (Zhang et al., 2016). Wang et al. prepared an ionic conductive solid electrolyte membrane for a solid-state Na- CO_2 battery by compositing $\text{Na}_{2.7}\text{Zr}_2\text{Si}_2\text{PO}_{11.7}\text{F}_{0.3}$ with PVDF-HFP matrix, which exhibited an ionic conductivity of up to $2.4 \times 10^{-4} \text{ S cm}^{-1}$ at room temperature (Wang et al., 2024). However, the ideal room-temperature ionic conductivity is still hard to realize in this stage. Besides the difficulty in this part, another significant challenge lies in the incompatible interfacial contact between electrodes and electrolytes, which induce large interfacial resistance and sluggish kinetics. The practical applications of NZSP-based CSSEs are inevitably hindered especially when these conditions are simultaneously involved. Clearly, further advances in the exploration of high-performance CSSEs-based SMBs are urgently needed to enable fast ionic transportation and enhanced interfacial stability.

Herein, we propose a functional and flexible CSSE based on ionically conductive $\text{Na}_{3.7}\text{Zr}_{1.45}\text{Sc}_{0.4}\text{Mg}_{0.15}\text{Si}_2\text{PO}_{12}$ (NSMZSP) inorganic filler and stable polyvinylidene fluoride (PVDF) organic matrix for high-performance SMBs. Both an ideal room-temperature ionic conductivity and superior electrolyte/electrodes interface compatibility can be concurrently achieved. Specifically, multiple three-dimensional ionic transport channels along the PVDF, NSMZSP, and PVDF/NSMZSP interfaces were effectively constructed to redistribute uneven Na^+ flux and enhance Na^+ transport kinetics, achieving improved room-temperature ionic conductivity ($5.5 \times 10^{-4} \text{ S cm}^{-1}$) and a high Na^+ transference number (0.56). Furthermore, the integrally synthesized composite network of the PVDF@NSMZSP CSSE combines the advantages of inorganic filler and organic matrix, exhibiting compatible interfacial contact between electrodes and electrolyte. With these merits, the obtained symmetric cells achieve a stable cycling property over 300 h at 1 mA cm^{-2} with cumulative capacity of 300 mAh cm^{-2} . When coupled with $\text{Na}_3\text{V}_2(\text{PO}_4)_3$ (NVP) cathode, the assembled full cell demonstrates outstanding capacity retention of 94.5% after 100 cycles with high average Coulombic efficiency at a mass loading of 3 mg cm^{-2} . This work highlights the unique design of CSSE, offering a new perspective for the practical applications of next-generation SMBs.

2 Experimental

2.1 Materials preparation

$\text{Na}_{3.7}\text{Zr}_{1.45}\text{Sc}_{0.4}\text{Mg}_{0.15}\text{Si}_2\text{PO}_{12}$ (NSMZSP) was fabricated by a standard solid-state reaction synthesis according to our previous study (Wang et al., 2025d). The obtained pellets were further milled at 300 rpm for 12 h to achieve homogeneous powder. Polyvinylidene fluoride (PVDF, Sigma-Aldrich), sodium bis(fluorosulfonyl)imide (NaFSI, Sigma-Aldrich) and $\text{Na}_3\text{V}_2(\text{PO}_4)_3$ (NVP, Sigma-Aldrich) were used before drying at 120 °C for 24 h under a vacuum to remove trace water. Carbon black, N-methyl-2-pyrrolidone (NMP), N, N-dimethylformamide (DMF) and sodium metal were purchased locally. The batteries (CR-2032 type) were purchased from Saibo electrochemical materials website in Taobao.

2.2 Preparation of the composite solid-state electrolytes

A certain amount of PVDF and NaFSI (Quality ratio is 3:2) was directly added in 5 mL N, N-dimethylformamide (DMF) to obtain a homogeneous slurry under vigorous stirring at 70 °C. Then, 0.75 g NSMZSP inorganic filler was added into the slurry with a continuous stirring for 12 h to prepare PVDF@NSMZSP composite solid-state electrolyte membrane (Zeng et al., 2025). After casting the homogenized slurry onto a glass plate using a 200 μm casting mould, it was transferred to a vacuum drying oven at 60 °C for 24 h to remove the solvent. The PVDF@NaFSI composite solid-state electrolyte without the addition of NSMZSP inorganic filler was also prepared under the same process. The obtained final composite solid-state electrolytes (CSSEs) had a thickness of approximately 90 μm.

2.3 Characterization

The crystal phase of the synthesized samples was analyzed using X-ray diffraction (XRD) with a PANalytical Aeris X-ray diffractometer with Cu Kα radiation ($\lambda = 1.5406 \text{ \AA}$) at a scanning rate of 2°/min. The morphological map of the surface and cross-section of samples were carried out by scanning electron microscopy (SEM, JEOL 7500 SEM). The chemical bond of CSSEs was determined by Fourier transform infrared spectroscopy (FT-IR, Spectrometer, Spectrum 3). X-ray photoelectron spectroscopy (XPS) characterization was performed on a Thermo Scientific Nexsa X-ray photoelectron spectrometer to characterize interactions between PVDF and NSMZSP, the Ar-protected sample injection was performed using a transition chamber through an Ar-filled glove box to avoid exposure to ambient air.

2.4 Electrochemical measurements

The Na//Cu, Na//Na and Na//NVP cells were assembled as CR2032 coin cells to measure the electrochemical performances. The Na₃V₂(PO₄)₃ (NVP) powder, carbon black, polyvinylidene fluoride (PVDF) with a weight ratio of 7:2:1 were mixed by N-methyl-2-pyrrolidone (NMP) to obtain a uniform slurry. The resulting slurry was then cast onto an aluminum foil current collector and dried for 12 h in a vacuum under 90 °C. The coated aluminum foil was punched into discs with a diameter of 6 mm and active mass loadings of near 1.5 or 3 mg cm⁻². Electrochemical impedance spectroscopy (EIS) tests and Chronoamperometry (CA) tests were recorded using the Biologic VMP3 electrochemical workstation. All the cells were galvanostatically charged and discharged using the LANDt battery testing system. The galvanostatic cycling of the full cells was characterized in the voltage of 2.5–3.8 V vs. Na/Na⁺ at room temperature (20 °C). The ionic conductivity of CSSEs was determined according to the Nyquist plot. The experiment was carried out with two stainless-steel (SS) sandwiching the CSSEs to construct SS//CSSEs//SS cells. The ionic conductivity (σ) is calculated based on the equation:

$$\sigma = \frac{L}{RS}$$

where L and S are the thickness and contact area of the PVDF@NaFSI and PVDF@NSMZSP membranes, and R points to the bulk resistance in the AC impedance spectrum.

The corresponding thermal activation energy (E_a) was derived from Arrhenius equation:

$$\sigma = A \exp\left(-\frac{E_a}{RT}\right)$$

where σ is the calculated ionic conductivity, A is the pre-exponential constant, T is the absolute temperature, and R is the standard gas constant. A series of temperatures of 20, 30, 40, and 50 °C were selected during the measurements.

The Na⁺ transference number (t_{Na^+}) for PVDF@NaFSI and PVDF@NSMZSP was measured in Na//CSSEs//Na cells at 20 °C, which was calculated according to the equation:

$$t_{Na^+} = \frac{I_S(\Delta V - I_0 R_0)}{I_0(\Delta V - I_S R_S)}$$

where I_0 and I_S refer to the initial and steady current, respectively, R_0 and R_S refer to the initial resistance and steady interfacial resistance obtained by EIS before and after the polarization, respectively, ΔV served as the applied potential of 10 mV.

2.5 COMSOL multiphysics simulations

The simulations of electric field distribution and Na⁺ ion concentration in PVDF@NaFSI and PVDF@NSMZSP CSSEs during Na deposition were conducted based on a finite element method (FEM) with the COMSOL Multiphysics software (Zheng et al., 2025). The physical models were defined by the law of mass conservation and electroneutrality assumption of related ions without considering the possible side reactions. A simulation model was built for a local model of 90*80 μm, the upper and lower boundaries were in contact with Na metal electrodes. A layer of array-arranged rectangular channels was set on the surface of the dendrite to represent the rectifying effect on the ion flow and electron flow. The simulation steps include a current distribution initialization and a steady step. The initial ion concentration is set to 1,500 mol m⁻³. The electrolyte conductivity is 0.1 S m⁻¹, and the boundary potential is 0.25V. During the deposition process, ions diffusing toward the surface of the depositing layer gain electrons and are reduced to Na atoms. As a result, the deposition layer gradually thickens and protrudes, accompanied by the continuous depletion of ions in the electrolyte. Consequently, the ion concentration at the deposition surface approaches 0, while the ion flux and electron density at the dendrite surface reach their maximum values.

3 Results and discussion

3.1 Synthesis process and morphological characterization

The homogeneous precursor solution consists of PVDF polymer matrix, NSMZSP inorganic filler, and sodium bis(fluorosulfonyl)

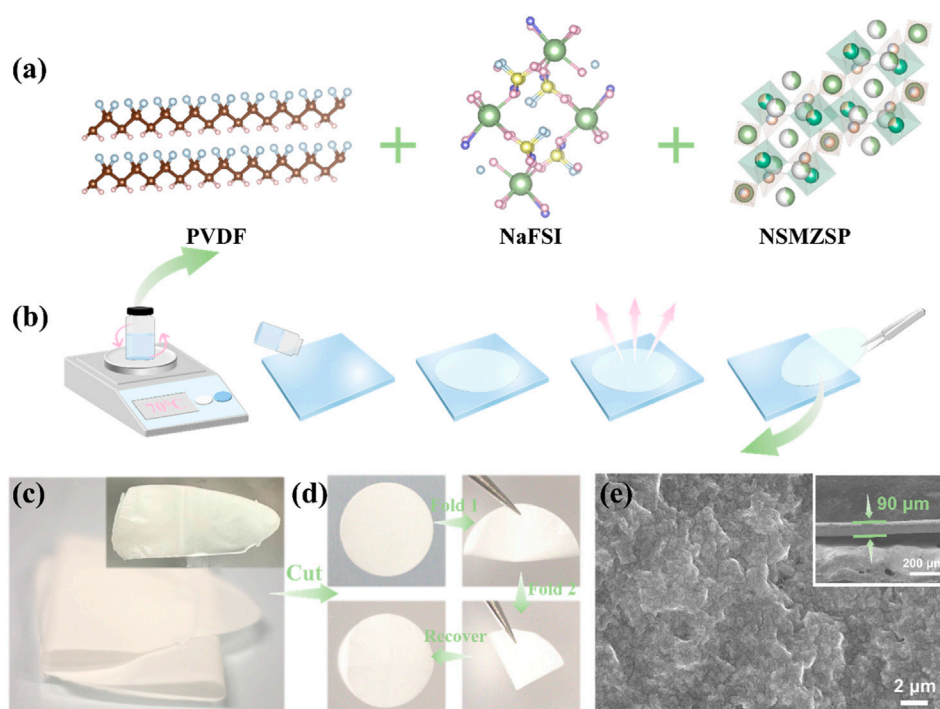


FIGURE 1 Synthesis process and morphological characterization. (a) Schematic illustrations of the PVDF, NaFSI, and NSMZSP structure. (b) Fabrication process of CSSEs. (c) Digital images of bendable PVDF@NSMZSP CSSE. (d) Folding test of PVDF@NSMZSP CSSE. (e) The top-view SEM image and inset cross-sectional SEM image of PVDF@NSMZSP CSSE.

imide (NaFSI) salt (Figure 1a). PVDF-based CSSEs are widely adopted owing to their flexibility, processability, and compatibility with scalable manufacturing processes, which can effectively dissociate NaFSI salts under vigorous stirring (Ling et al., 2025). NSMZSP with high ionic conductivity and excellent chemical stability was fabricated by a standard solid-state reaction synthesis according to our previous study (Wang et al., 2025d). An extra ball-milling process was performed to obtain uniform NSMZSP powder, which is indexed to the standard rhombohedral Na₃Zr₂Si₂PO₁₂ phase (Zou et al., 2020). Supplementary Figure S1 shows scanning electron microscope (SEM) images of obtained NSMZSP samples with homogenous grain size distribution. A facile solution casting method was utilized to improve the transmission efficiency of Na⁺ within the composite membrane and promote uniform Na⁺ deposition. As depicted in Figure 1b, the NSMZSP-based slurry was cast into a glass mold and thermally evaporated to create a dense, uniform membrane. The as-obtained flexible PVDF@NSMZSP CSSE can be rolled randomly without any detachment or cracking, and the cut membrane retains its original shape even after two folds, with no shedding or damage, indicating the sufficient flexibility and high mechanical stability, thereby facilitating reliable battery assembly and resisting dendrite penetration (Figures 1c,d) as shown in the microscopic morphology of PVDF@NSMZSP CSSE in Figure 1e, the top-view SEM image demonstrate that the PVDF@NSMZSP membrane is thin, dense, and free from macroscopic defects. Inset cross-sectional SEM image exhibits that the NSMZSP inorganic filler is well-integrated into PVDF polymer matrix with an approximate thickness of 90 μm (Figure 1e;

Supplementary Figure S3a). While for the synthesized PVDF@NaFSI membrane, a relatively loose morphology with various degrees of structural defects can be observed, which may serve as undesirable pathways for dendrite penetration and propagation (Supplementary Figure S2,S3b). Consequently, the Na⁺ ion transport across the CSSE becomes discontinuous, leading to inhomogeneous Na⁺ deposition and deteriorated interfacial stability during cycling. These results demonstrate the successful synthesis of PVDF@NSMZSP CSSE with high mechanical strength and dense conductive structure, which make it possible for SMBs with enhanced safety and stability.

3.2 Structural and functional characterization

The structural evolution and functional application of PVDF@NSMZSP CSSE were systematically investigated through multi-scale characterization. The X-ray diffraction (XRD) was carried out to investigate the structural evolution induced by NSMZSP inorganic filler. As shown in Figure 2a, all components of NSMZSP (dark grey spots) are well integrated into PVDF polymer matrix without losing their crystalline structure. Regarding the PVDF structure (pink spots), compared with the pure PVDF matrix, a diminished intensity of the 18.5° (020) peak in PVDF@NSMZSP CSSE can be observed. This attenuation suggests suppression of the α-phase, indicating that the PVDF@NSMZSP restrains the formation of non-polar crystalline domains (Yang et al., 2024). Simultaneously, the dominant 20.3° (110/200) peak remains sharp in PVDF@NSMZSP

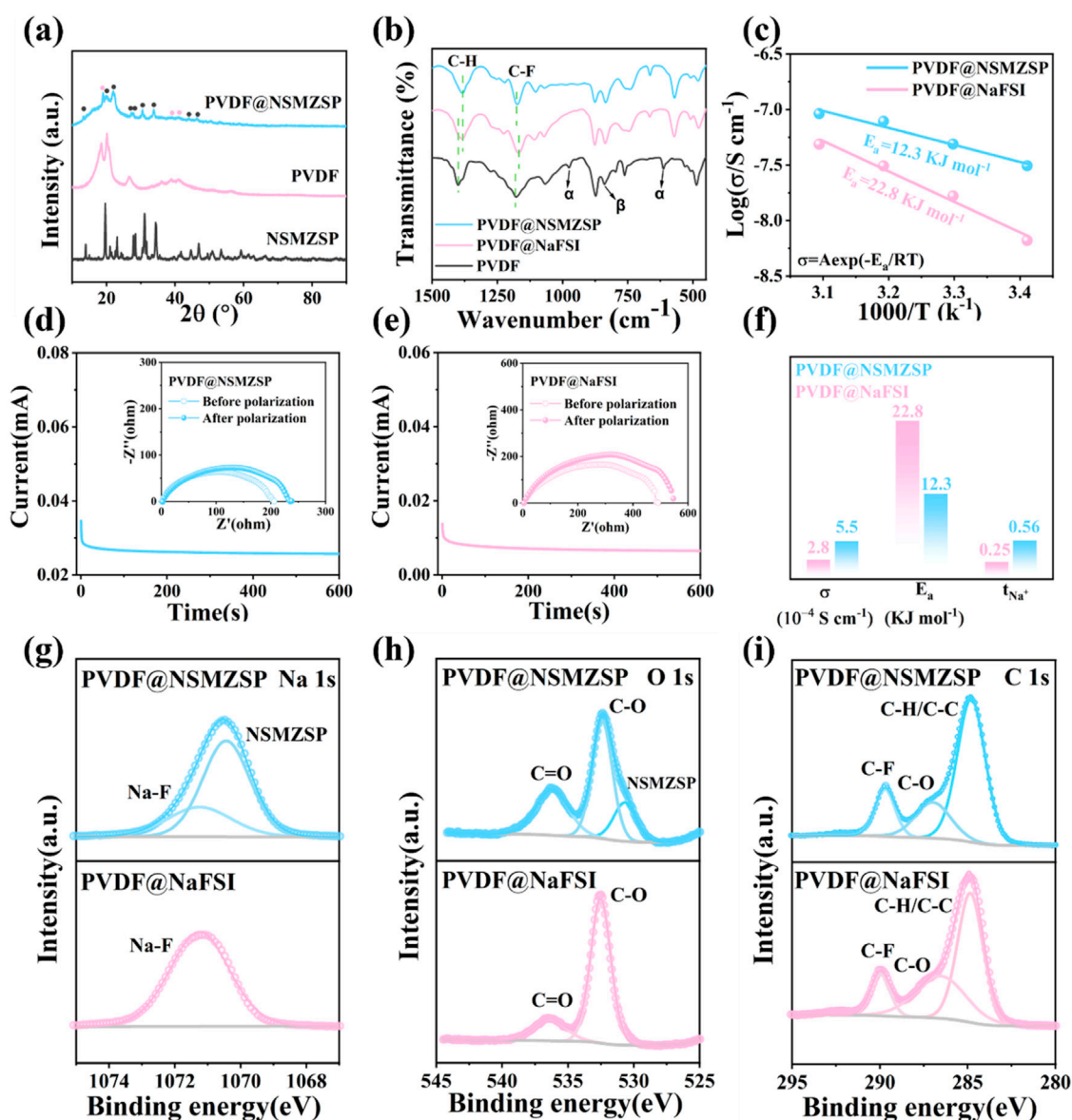


FIGURE 2 Structural and functional characterization. (a) XRD patterns of NSMZSP powder, PVDF@NSMZSP, and PVDF@NaFSI CSSEs. (b) FT-IR spectra of PVDF powder, PVDF@NSMZSP, and PVDF@NaFSI CSSEs. (c) Arrhenius plots of ionic conductivities for SS//PVDF@NSMZSP//SS and SS//PVDF@NaFSI//SS cells. Polarization curve of (d) Na//PVDF@NSMZSP//Na cell and (e) Na//PVDF@NaFSI//Na cell. The inset is EIS spectra before and after polarization. (f) Comparisons of σ , E_a , and t_{Na^+} between PVDF@NSMZSP and PVDF@NaFSI CSSEs. XPS spectra of (g) Na 1s, (h) O 1s, and (i) C 1s in PVDF@NSMZSP and PVDF@NaFSI CSSEs.

CSSE, reflecting the enhancement of the polar β -phase, indicating the superior dispersion of NSMZSP in the PVDF matrix without disrupting long-range atomic order (Luo et al., 2025; Zhou et al., 2022). The overall left-shift of diffraction peaks in the PVDF@NSMZSP CSSE, relative to both pristine PVDF and NSMZSP, indicates a lattice expansion and structural relaxation induced by strong interfacial interactions between polymer matrix and inorganic filler. Such structural modulation is favorable for enhancing polymer-ceramic compatibility and facilitating Na^+ ions transport. Fourier transform infrared spectroscopy (FT-IR) spectra (Figure 2b) exhibits that a distinct shift of the C-H stretching vibration from $1,400\text{ cm}^{-1}$ to $1,385\text{ cm}^{-1}$ in both PVDF@NSMZSP

and PVDF@NaFSI CSSEs, which arises from the electrostatic interactions between Na^+ ions and the fluorine atoms or dipolar segments ($-CF_2-$) within the PVDF polymer matrix. Such interactions polarize the local electron cloud, thereby decreasing the electron density of adjacent C-H bonds, weakening their bond force constants, and consequently lowering the C-H vibrational frequency, which results in a rightward peak shift. For the C-F bonds, no obvious change is observed after the incorporation of NSMZSP into PVDF@NaFSI CSSE. This is because Na^+ ions preferentially accumulate or are adsorbed at the PVDF/NSMZSP interfaces, where the coordination between Na^+ and fluorine atoms enhances the polarization of C-F bonds. This enhanced polarization

compensates for the local polarization effect, leading to a negligible net spectral shift (Ayyaru et al., 2020). Moreover, the introduction of Na⁺ ions induces a phase transition of PVDF from the α -phase to the β -phase, as evidenced by the enhanced β -phase characteristic peak at 840 cm⁻¹ and the almost complete disappearance of the α -phase peaks at 975 cm⁻¹ and 612 cm⁻¹ in both PVDF@NSMZSP and PVDF@NaFSI CSSEs. The β -phase PVDF, owing to its high dipole moment and strong polarization capability, facilitates the dissociation of Na salts and promotes the formation of more continuous ionic transport pathways. These findings are well consistent with XRD analysis, confirming the construction of multiple ionic transport channels along the PVDF, NSMZSP, and PVDF/NSMZSP interfaces, thereby offering great potential in enhancing Na⁺ transport kinetics.

For high-performance energy storage systems, an ideal CSSE is required to be multifunctional, which can possess high room-temperature ionic conductivity, a broad electrochemical stability window, a high Na⁺ transference number, and intimate electrode/electrolyte interfacial contact to ensure efficient charge transfer and stable operation. To assess the ionic conductivity, electrochemical impedance spectroscopy (EIS) tests were conducted at various temperatures (20, 30, 40, 50 °C) in symmetric stainless-steel (SS)//CSSEs//SS cells. As shown in Supplementary Figure S4, the PVDF@NaFSI CSSE exhibits a relatively low room-temperature ionic conductivity (2.8×10^{-4} S cm⁻¹). Whereas the PVDF@NSMZSP CSSE achieves an enhanced room-temperature ionic conductivity of 5.5×10^{-4} S cm⁻¹, which is two times higher than the pristine one. Further analysis of PVDF@NSMZSP and PVDF@NaFSI CSSEs across temperatures demonstrates a linear Arrhenius relationship between ionic conductivity and temperature (Figure 2c). Notably, the activation energy (E_a) with the PVDF@NSMZSP CSSE was calculated to be 12.3 kJ mol⁻¹, which is much lower than that with the PVDF@NaFSI CSSE (22.8 kJ mol⁻¹), indicating a lower energy barrier for Na⁺ ions transfer. To determine the exact Na⁺ transference number, chronoamperometry with a constant potential step of 10 mV and EIS measurements at room temperature were measured, the t_{Na^+} value was subsequently calculated according to the Bruce-Vincent-Evans equation (Zheng et al., 2021). As depicted in Figures 2d,e, the t_{Na^+} value of PVDF@NSMZSP CSSE stands at 0.56, significantly exceeding that of the PVDF@NaFSI CSSE (0.25), indicating a correspondingly reduced migration of anions, thereby minimizing concentration polarization during cycling and enabling rapid Na⁺ migration (Liu et al., 2025). The calculated Na⁺ transference numbers are detailed in Supplementary Table S1. Notably, the PVDF@NSMZSP CSSE exhibits a higher room-temperature ionic conductivity, lower activation energy, and higher Na⁺ transference number, revealing its superior ability for fast Na⁺ ionic transport (Figure 2f).

X-ray photoelectron spectroscopy (XPS) was used to examine surface composition variations. In the Na 1s spectra (Figure 2g), PVDF@NaFSI exhibits a single Na-F peak, indicating the presence of Na⁺ mainly from the NaFSI salt. PVDF@NSMZSP exhibits an additional component corresponding to the NSMZSP phase, suggesting that Na⁺ interacts with the NSMZSP inorganic filler and participates in interfacial coordination, which facilitates continuous Na⁺ transport pathways (Li et al., 2025). The O 1s spectra (Figure 2h) displays two peaks at ~532.6 eV (C-O) and

~536.4 eV (C=O) in PVDF@NaFSI, while an additional peak associated with NSMZSP appears in PVDF@NSMZSP CSSE, reflecting the contribution of metal-oxygen bonds (Zr-O, Si-O, P-O) and indicating strong interfacial coupling between the organic matrix and inorganic filler (Su et al., 2025; Liao et al., 2025). In the C 1s spectra (Figure 2i), both CSSEs contain characteristic peaks of C-F, C-O, and C-H/C-C bond. PVDF@NSMZSP exhibits a decreased C-F and enhanced C-O intensity, implying increased chain polarization and partial substitution or interaction of C-F with the filler surface (Hu et al., 2025a). These results confirm that the incorporation of NSMZSP induces stronger interfacial interactions and enhances the dipole polarization of PVDF, thereby promoting Na salt dissociation and the formation of more continuous ionic transport channels. Similar results can be achieved from N 1s, S 2p, and F 1s spectra in Supplementary Figure S5, and the XPS studies of Zr, Si, P, Sc, Mg elements from NSMZSP inorganic filler are also shown in Supplementary Figure S6 accordingly (Thapaliya et al., 2023; Fan et al., 2024).

3.3 Sodium metal compatibility and stability

To evaluate the interface compatibility and Na plating/stripping stability of CSSEs against Na Metal, Na//Cu half cells among PVDF@NSMZSP and PVDF@NaFSI CSSEs were assembled to measure the Coulombic efficiency (CE). As shown in Figure 3a, the average CE of Na plating/stripping for PVDF@NSMZSP CSSE was recorded at an impressive value of 98.7% under full deposition conditions at a current density of 5 mA cm⁻² and a capacity of 1 mAh cm⁻², respectively. In contrast, the PVDF@NaFSI CSSE exhibits significant fluctuation in CE and can only maintain 100 cycles. The Na//PVDF@NSMZSP//Cu cell shows remarkable CE values and longevity (over 200 cycles), indicating the advantages of the PVDF@NSMZSP CSSE in suppressing Na dendrite formation while enhancing Na⁺ utilization rates. Furthermore, the charge and discharge curves at the 50th and 100th cycles in Figure 3b present that the Na//PVDF@NSMZSP//Cu cell displays a smaller voltage hysteresis with enhanced electrochemical deposition. While for the Na//PVDF@NaFSI//Cu cell, a large voltage hysteresis and obvious fluctuations can be detected, arising from the depletion of both CSSE and Na metal (Li et al., 2019). To further evaluate the cycling stability of CSSEs against Na metal, symmetric Na//Na cells among PVDF@NSMZSP and PVDF@NaFSI CSSEs were assembled for galvanostatic cycling tests at a current density of 1 mA cm⁻². As shown in Figures 3c,d, Na//PVDF@NSMZSP//Na cell presents an exceptional Na plating/stripping cycle performance, maintaining a stable voltage profile for over 300 h. The great cycling stability demonstrates the impressive compatibility of Na electrodes/CSSE and rapid Na⁺ ions migration at the interface. In contrast, Na//PVDF@NaFSI//Na cell exhibits constant voltage fluctuations during the whole cycling time, which is resulted from the continuous consumption of CSSE and Na dendrite growth. EIS measurement at room temperature was conducted to provide more insight on battery performance. Figures 3e,f present the EIS spectra of Na//Na cells among PVDF@NaFSI and PVDF@NSMZSP CSSEs before and after 100 h cycling, respectively. The resistances were extracted by fitting the impedance spectra using the inset equivalent circuit, where the initial point of the spectra corresponded to the

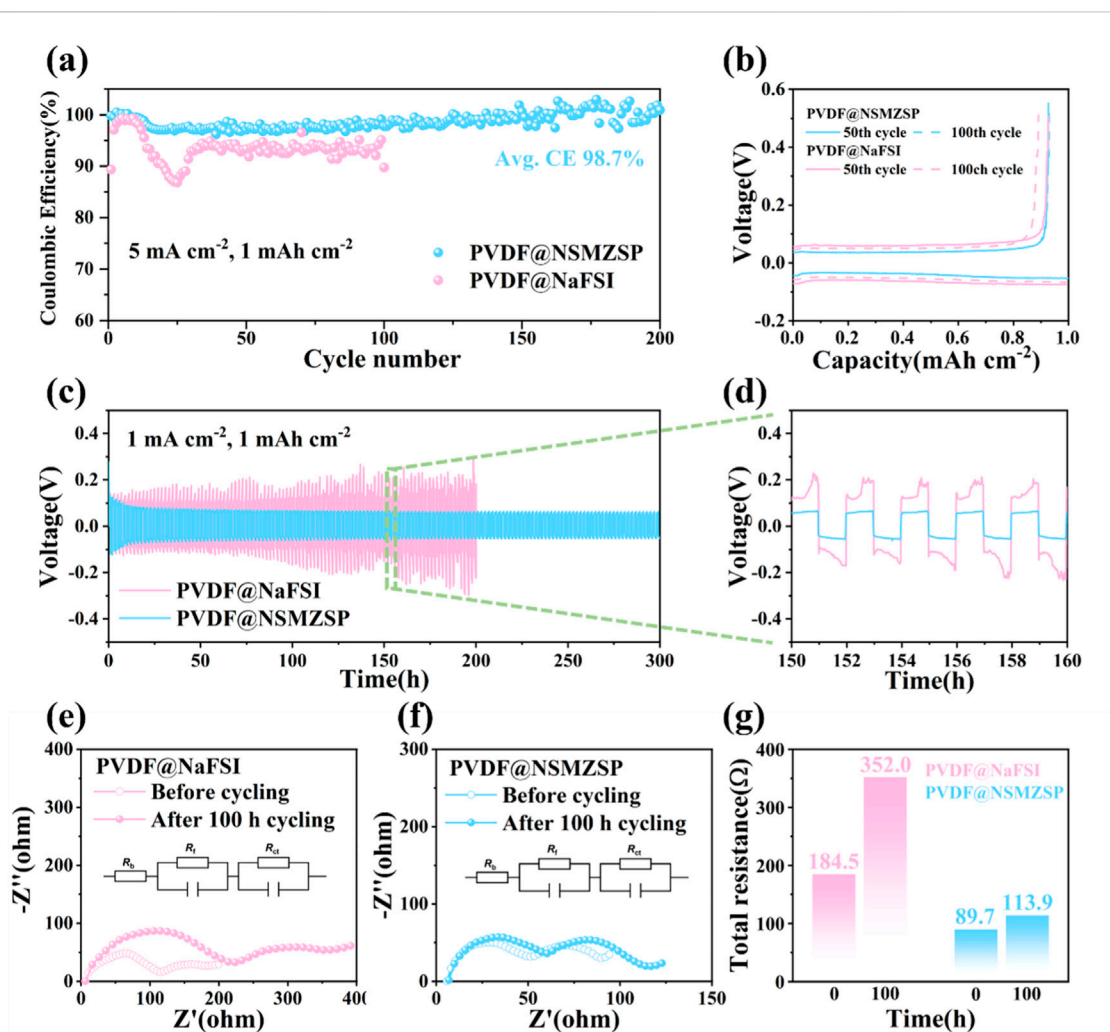


FIGURE 3

Sodium metal compatibility and stability. (a) Variations of Coulombic Efficiency with cycle numbers in Na//Cu half cells among PVDF@NSMZSP and PVDF@NaFSI CSSEs at 5 mA cm^{-2} , 1 mAh cm^{-2} . (b) Charge and discharge voltage profiles of Na//Cu half cells at 50th and 100th cycles. (c) Na plating/stripping voltage profile in Na//Na symmetric cells among PVDF@NSMZSP and PVDF@NaFSI CSSEs at 1 mA cm^{-2} , 1 mAh cm^{-2} . (d) Partial enlarged image of Na plating/stripping voltage profile in Na//Na symmetric cells. Time-resolved Nyquist plots in Na//Na symmetric cells among (e) PVDF@NaFSI and (f) PVDF@NSMZSP CSSEs at room temperature. (g) Total resistances in Na//Na symmetric cells calculated from EIS spectra.

resistance of the bulk electrolyte (R_b), the following semicircle corresponded to the interfacial resistance (R_f), and charge transfer resistance R_{ct} (Rao et al., 2021). The specific values of resistances are shown in Supplementary Table S2. The total resistance of the Na//PVDF@NSMZSP//Na cell remains stable and increases from $89.7 \text{ } \Omega$ to $113.9 \text{ } \Omega$ after 100 h cycling, which suggests that the PVDF@NSMZSP CSSE forms a stable interface with Na metal, effectively suppressing dendrite growth and preventing severe side reactions. The continuous Na^+ transport pathways maintain fast ion migration kinetics, the gradual formation of a stable interphase during the early cycles contributes to the steady and benign impedance evolution. While for the Na//PVDF@NaFSI//Na cell, the total resistance dramatically increases from an initial value of $184.5 \text{ } \Omega$ – $352.0 \text{ } \Omega$, exhibiting unsatisfied battery performance (Figure 3g). Given these features, PVDF@NSMZSP CSSE demonstrates considerable Na metal compatibility and cycling stability for constructing high-performance SMBs.

3.4 Full cell electrochemical performance with $\text{Na}_3\text{V}_2(\text{PO}_4)_3$ cathode

Na//NVP cathode full cells were assembled with PVDF@NSMZSP and PVDF@NaFSI CSSEs to assess practical performance (Wu et al., 2025). The galvanostatic charge/discharge profiles of the Na//PVDF@NSMZSP//NVP cell at a current rate of 0.5 C are presented in Figure 4a, where the 1st, 10th, 50th, 100th, and 200th cycles within the voltage range of 2.5 – 3.8 V (vs. Na^+/Na) are displayed. Nearly overlapping charge/discharge curves indicate stable cycling behavior, with the cell delivering an initial discharge capacity of 95.6 mAh g^{-1} . For comparison, the corresponding galvanostatic profiles of the Na//PVDF@NaFSI//NVP cell are provided in Supplementary Figure S7. The long-term cycling stability of the Na//PVDF@NSMZSP//NVP cell at 0.5 C is presented in Figure 4b. The Na//PVDF@NSMZSP//NVP cell delivers a discharge capacity of 91.6 mAh g^{-1} and maintains an excellent capacity retention of 95.8% after 200 cycles at room

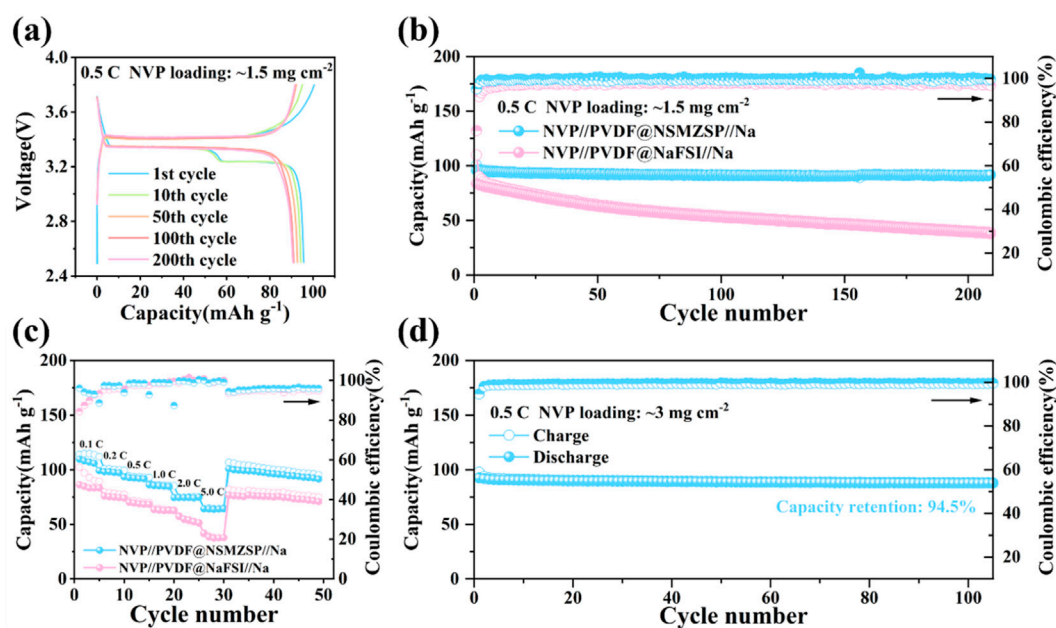


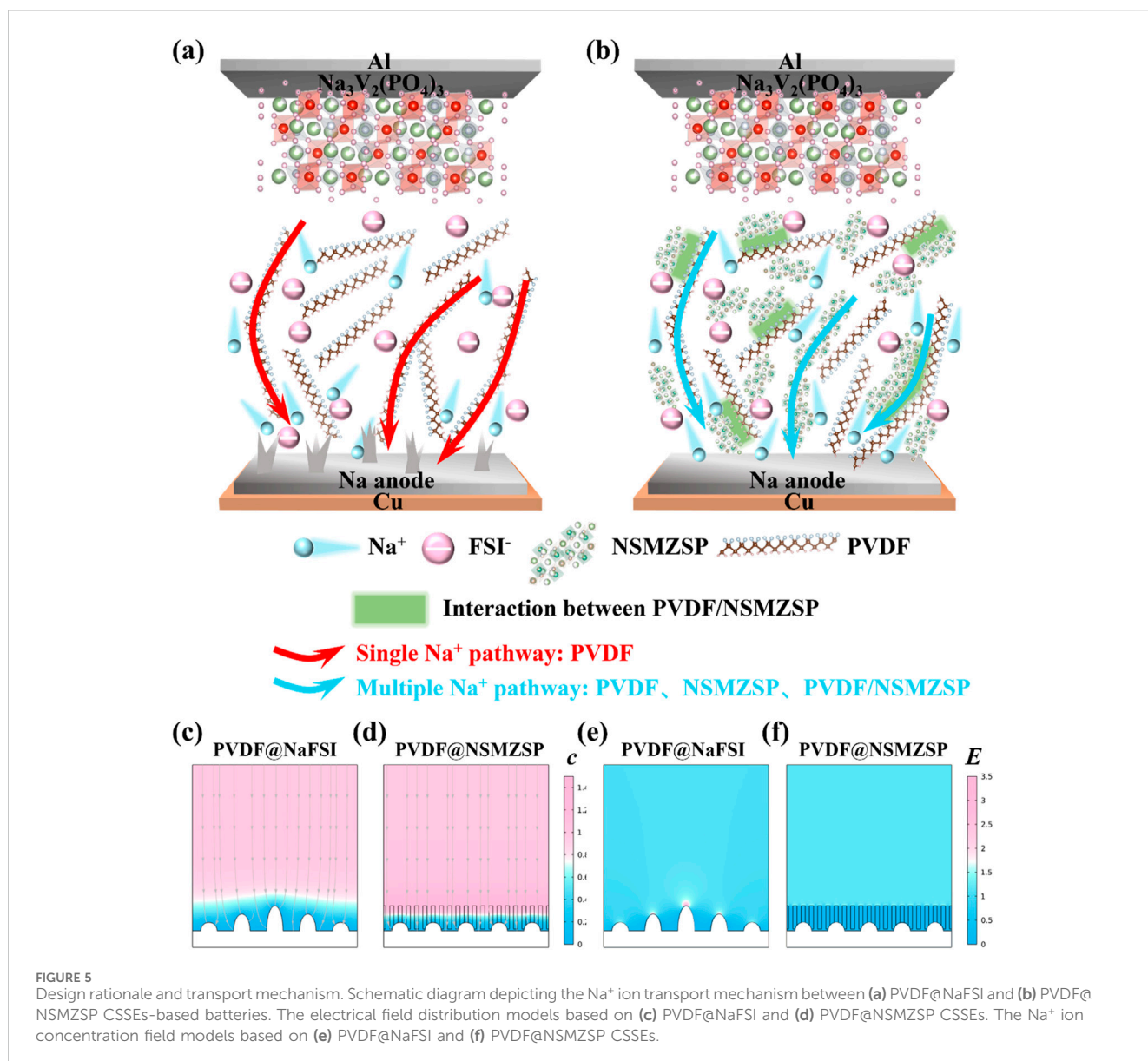
FIGURE 4 Full cell electrochemical performance with $\text{Na}_3\text{V}_2(\text{PO}_4)_3$ cathode. (a) Galvanostatic charge/discharge cycling profile for the selected cycles at the rate of 0.5 C. (b) Long-term cycling stability at 0.5 C with NVP loading of $\sim 1.5 \text{ mg cm}^{-2}$. (c) Rate performance in the range of 0.1–5 C at room temperature. (d) Cycling durability at 0.5 C with NVP loading of $\sim 3 \text{ mg cm}^{-2}$.

temperature. Such outstanding electrochemical stability can be ascribed to the well-engineered PVDF, NSMZSP, and PVDF/NSMZSP interfaces, which ensure intimate and compatible contact between the electrodes and CSSE. This structural integration promotes rapid interfacial charge-transfer kinetics, effectively suppressing pore or void formation and thereby mitigating dendrite propagation. In contrast, the Na//PVDF@NaFSI//NVP cell suffers from evident capacity degradation and poor cycling stability, delivering only 37.7 mAh g^{-1} , which is associated with severe Na dendrite growth at the CSSE/electrodes interface. The rate performance of these cells can be observed in Figure 4c. The Na//PVDF@NSMZSP//NVP cell demonstrates outstanding rate capability under gradually increased current densities ranging from 0.1 to 5 C (1 C $\approx 117.6 \text{ mA g}^{-1}$), with each rate maintained for five cycles. At 0.1 C, the cell delivers an initial charge/discharge capacity of $114.2/109.7 \text{ mAh g}^{-1}$, corresponding to a high CE of 96.1%. Even when operated at a high rate of 5 C, a reversible capacity of 64.2 mAh g^{-1} is still achieved, highlighting excellent kinetic performance. Remarkably, when the current density is reverted to 0.1 C after five cycles at 5 C, the charge/discharge curves nearly overlap with those of the initial low-rate cycles, maintaining a stable reversible capacity of 100.8 mAh g^{-1} . Moreover, to evaluate whether the PVDF@NSMZSP CSSE can still perform well under practical, high-energy conditions, a high mass loading of NVP cathode ($\sim 3 \text{ mg cm}^{-2}$) was utilized to demonstrate the feasibility. As shown in Figure 4d, the Na//PVDF@NSMZSP//NVP cell exhibits an initial discharge capacity of 92.5 mAh g^{-1} at 0.5 C, an exceptional capacity retention as 94.5% over 100 cycles at room temperature can be achieved. A performance comparison between the PVDF@NSMZSP CSSE developed in this study and previously reported NZSP inorganic filler-based CSSEs was

summarized in Supplementary Table S3, with detailed information on ionic conductivity, E_a , t_{Na^+} , and electrochemical performance. The optimized PVDF@NSMZSP CSSE is superior among other NZSP inorganic filler-based CSSEs, highlighting the enhancement of the ionic conductivity and interfacial compatibility. With these electrochemical characterizations, the novel PVDF@NSMZSP CSSE holds substantial advantages in comprehensive performance, specifically in terms of efficient Na^+ transport, robust cycle stability, and high-rate capability.

3.5 Design rationale and transport mechanism

These findings confirm that multiple ionic transport channels along the PVDF, NSMZSP, and PVDF/NSMZSP interfaces have been successfully established in PVDF@NSMZSP CSSE, facilitating rapid Na^+ ionic transport and superior room-temperature ionic conductivity. The consistent electrochemical results demonstrate excellent electrode-electrolyte compatibility and stable Na^+ migration pathways. Figures 5a,b exhibit the schematic diagram of the Na^+ ion transport mechanism between PVDF@NaFSI and PVDF@NSMZSP CSSEs-based batteries. Specifically, for the PVDF@NaFSI-based battery, the PVDF polymer matrix with NaFSI salt is considered as the only pathway for Na^+ ionic transport, Na^+ tends to aggregate around FSI⁻ anions and presents anisotropic distribution when passing through CSSE. Consequently, the large diffusion energy barrier induces uneven Na^+ deposition and dynamic contact instability, leading to serious dendrite growth and side reactions. In contrast, with the incorporation with NSMZSP inorganic filler, PVDF@NSMZSP-



based battery exhibits multiple ionic transport channels along the PVDF, NSMZSP, and PVDF/NSMZSP interfaces, effectively broadening additional Na⁺ migration pathways and accelerating Na⁺ ionic transport, thus redistributing the uneven Na⁺ flux from pristine PSSE and suppressing the formation of Na⁺ concentration gradient. To further confirm these effects, COMSOL finite-element simulations were employed to investigate the rationale of PVDF@NSMZSP CSSE in regulating the electric field distribution and Na⁺ concentration distribution (Hu et al., 2025b). As illustrated in Figure 5c, the Na surface exhibits a nonuniform electric field when employing the PVDF@NaFSI CSSE, where regions with locally intensified field strength act as preferential sites for Na⁺ deposition, eventually inducing Na dendrite growth. In contrast, the PVDF@NSMZSP CSSE generates a well-distributed electric field across the Na surface (Figure 5d). Moreover, as depicted in Figures 5e,f, the PVDF@NSMZSP CSSE enables a considerably more uniform Na⁺ flux compared to that in PVDF@NaFSI CSSE. These simulation results are well consistent with the aforementioned functional characterizations and comprehensive

electrochemical performances, collectively demonstrate that the incorporation of the NSMZSP inorganic filler effectively homogenizes both the electric field and the Na⁺ concentration distribution, thereby enhancing the reversibility and stability of the practical SMBs.

4 Conclusion

In summary, this work presents a facile strategy to construct a novel PVDF@NSMZSP CSSE for high-performance SMBs. Experimental and theoretical analysis demonstrate a superior room-temperature ionic conductivity of $5.5 \times 10^{-4} \text{ S cm}^{-1}$ and a high Na⁺ transference number of 0.56. The formation of multiple ionic transport channels within the CSSE can effectively broaden Na⁺ migration pathways and enhance Na⁺ transport kinetics. A galvanostatic Na//Na symmetric cell employing PVDF@NSMZSP CSSE exhibits ultra-stable Na plating/stripping cycling performance for over 300 h at 1 mA cm^{-2} , underscoring its rapid Na⁺ migration

and excellent electrolyte/electrode compatibility. Moreover, a Na//PVDF@NSMZSP//NVP full cell with a high cathode mass loading ($\sim 3 \text{ mg cm}^{-2}$) achieves an exceptional capacity retention of 94.5% over 100 cycles at 0.5 C, highlighting its strong potential for practical high-energy-density SMBs. Overall, this work offers innovative insights into the rational design of composite solid-state electrolytes with enhanced Na^+ transport kinetics and interface compatibility, significantly advancing the development of sodium-based energy storage technologies.

Data availability statement

The original contributions presented in the study are included in the article/[Supplementary Material](#), further inquiries can be directed to the corresponding authors.

Author contributions

XW: Visualization, Formal Analysis, Data curation, Writing – review and editing, Writing – original draft, Conceptualization, Investigation, Methodology. JL: Writing – review and editing, Investigation, Software, Conceptualization. XL: Investigation, Writing – review and editing, Data curation. HL: Writing – review and editing, Investigation. ZT: Data curation, Investigation, Writing – review and editing. WP: Funding acquisition, Writing – review and editing, Project administration, Supervision, Conceptualization, Investigation. BJ: Project administration, Writing – review and editing, Supervision, Conceptualization, Funding acquisition, Investigation.

Funding

The authors declare that financial support was received for the research and/or publication of this article. This work was supported by the Australian Research Council (ARC) for DP230100198.

Acknowledgements

X. W is grateful for the sponsorship from China Scholarship Council (202209040008). The authors acknowledge support

References

- Armand, M., and Tarascon, J. M. (2008). Building better batteries. *Nature* 451 (7179), 652–657. doi:10.1038/451652a
- Ayyaru, S., Dinh, T. T. L., and Ahn, Y.-H. (2020). Enhanced antifouling performance of PVDF ultrafiltration membrane by blending zinc oxide with support of graphene oxide nanoparticle. *Chemosphere* 241, 125068. doi:10.1016/j.chemosphere.2019.125068
- Bay, M.-C., Wang, M., Grissa, R., Heinz, M. V. F., Sakamoto, J., and Battaglia, C. (2020). Sodium plating from $\text{Na-}\beta''\text{-Alumina}$ ceramics at room temperature, paving the way for fast-charging all-solid-state batteries. *Adv. Energy Mater.* 10 (3), 1902899. doi:10.1002/aenm.201902899
- Dong, Z. L., Gan, Y., Martins, V., Wang, X., Fu, B., Jin, E., et al. (2025). Novel sulfide-chloride solid-state electrolytes with tunable anion ratio for highly stable solid-state sodium-ion batteries. *Adv. Mater.* 37 (30), 2503107. doi:10.1002/adma.202503107

from the Australian Research Council (ARC) for DP230100198. B. J acknowledges an ongoing Honorary Professorial Fellowship at the University of Wollongong, which provides a platform to supervise students and lead collaborative research efforts.

Conflict of interest

The authors declare that the research was conducted in the absence of any commercial or financial relationships that could be construed as a potential conflict of interest.

The author(s) declared that they were an editorial board member of *Frontiers*, at the time of submission. This had no impact on the peer review process and the final decision.

Generative AI statement

The authors declare that no Generative AI was used in the creation of this manuscript.

Any alternative text (alt text) provided alongside figures in this article has been generated by *Frontiers* with the support of artificial intelligence and reasonable efforts have been made to ensure accuracy, including review by the authors wherever possible. If you identify any issues, please contact us.

Publisher's note

All claims expressed in this article are solely those of the authors and do not necessarily represent those of their affiliated organizations, or those of the publisher, the editors and the reviewers. Any product that may be evaluated in this article, or claim that may be made by its manufacturer, is not guaranteed or endorsed by the publisher.

Supplementary material

The Supplementary Material for this article can be found online at: <https://www.frontiersin.org/articles/10.3389/fbael.2025.1734762/full#supplementary-material>

- Du, L., Xu, G., Sun, C., Zhang, Y.-H., Zhang, H., Dong, T., et al. (2025). Smart gel polymer electrolytes enlightening high safety and long life sodium ion batteries. *Nat. Commun.* 16 (1), 2979. doi:10.1038/s41467-025-57964-7
- Dutra, A. C. C., Goldmann, B. A., Islam, M. S., and Dawson, J. A. (2025). Understanding solid-state battery electrolytes using Atomistic modelling and machine learning. *Nat. Rev. Mater.* 10 (8), 566–583. doi:10.1038/s41578-025-00817-y
- Famprikis, T., Canepa, P., Dawson, J. A., Islam, M. S., and Masquelier, C. (2019). Fundamentals of inorganic solid-state electrolytes for batteries. *Nat. Mater.* 18 (12), 1278–1291. doi:10.1038/s41563-019-0431-3
- Fan, W., Wang, W., Xie, Q., He, X., Li, H., Zhao, J., et al. (2024). A sodium bis(fluorosulfonyl)imide (NaFSI)-based multifunctional electrolyte stabilizes the performance of $\text{NaNi}_{1/3}\text{Fe}_{1/3}\text{Mn}_{1/3}\text{O}_2/\text{hard carbon}$ sodium-ion batteries. *Chem. – A Eur. J.* 30 (43), e202401321. doi:10.1002/chem.202401321

- Fan, Y., Wang, X., Bo, G., Xu, X., See, K. W., Johannessen, B., et al. (2025). Operando synchrotron X-Ray absorption spectroscopy: a key tool for cathode material studies in next-generation batteries. *Adv. Sci.* 12 (10), 2414480. doi:10.1002/advs.202414480
- Hu, Z., Liu, L., Wang, X., Zheng, Q., Han, C., and Li, W. (2024). Current progress of anode-free rechargeable sodium metal batteries: origin, challenges, strategies, and perspectives. *Adv. Funct. Mater.* 34 (22), 2313823. doi:10.1002/adfm.202313823
- Hu, Z., Liu, L., Wang, X., Zheng, Q., Lu, H., Tang, Z., et al. (2025a). Enhancing low-temperature durability and sodium-ion transport of anode-free sodium metal batteries through utilization of a solvent adsorption separator. *Energy & Environ. Sci.* 18, 10048–10060. doi:10.1039/d5ee03213j
- Hu, Z., Liu, L., Wang, X., Lu, H., Zheng, Q., Gao, Y., et al. (2025b). *In situ* integration of rapid ion-diffusion interlayers on Cu current collectors toward ultrafast anode-free sodium metal batteries. *ACS Nano* 19 (25), 23193–23208. doi:10.1021/acsnano.5c05043
- Huang, J., Wu, K., Xu, G., Wu, M., Dou, S., and Wu, C. (2023). Recent progress and strategic perspectives of inorganic solid electrolytes: fundamentals, modifications, and applications in sodium metal batteries. *Chem. Soc. Rev.* 52 (15), 4933–4995. doi:10.1039/d2cs01029a
- Huang, Z., Wang, S., Guo, X., Marlon, F., Fan, Y., Pang, W.-K., et al. (2024). High-entropy layered oxide cathode materials with moderated interlayer spacing and enhanced kinetics for sodium-ion batteries. *Adv. Mater.* 36 (50), 2410857. doi:10.1002/adma.202410857
- Huang, J., An, X., Cheng, Z., Li, L., Dou, S.-X., Liu, H.-K., et al. (2025). Dipole-dipole interaction-induced dense primitive solid-electrolyte interphase for high-power Ah-level anode-free sodium metal batteries. *Nat. Commun.* 16 (1), 8586. doi:10.1038/s41467-025-63593-x
- Li, M., Lu, J., Chen, Z., and Amine, K. (2018). 30 years of lithium-ion batteries. *Adv. Mater.* 30 (33), 1800561. doi:10.1002/adma.201800561
- Li, C., Liu, S., Shi, C., Liang, G., Lu, Z., Fu, R., et al. (2019). Two-dimensional molecular brush-functionalized porous bilayer composite separators toward ultrastable high-current density lithium metal anodes. *Nat. Commun.* 10 (1), 1363. doi:10.1038/s41467-019-09211-z
- Li, Y., Hosaka, T., Maibach, J., and Johansson, P. (2025). Stable anode interphase enabled use of protic electrolytes in sodium metal batteries. *Energy Storage Mater.* 82, 104566. doi:10.1016/j.ensm.2025.104566
- Liao, H., Chen, K., Wang, X., Liu, F., He, X., Tong, J., et al. (2025). Selective sulfuration suppressed iron leakage in nickel-iron catalyst to stimulate double lattice oxygen for efficient water oxidation. *Adv. Funct. Mater.* 35 (n/a), 2506656. n/a. doi:10.1002/adfm.202506656
- Ling, Q.-C., Chen, D.-C., Zhu, X., Zhu, Y.-F., Hong, Z.-Z., Liu, J., et al. (2025). Probing local asymmetric site anchored anion based on multifunctional polymer electrolyte for sustainable solid-state sodium-metal battery. *Adv. Mater.* (n/a), e14352. n/a. doi:10.1002/adma.202514352
- Liu, Q., An, Q., Zeng, K., Yang, M., Zhu, H., Liang, X., et al. (2025). Tuning electronic structure of MOF-based solid-state electrolytes to activate dormant lithium and facilitate ion transport kinetics towards lithium metal batteries. *Energy & Environ. Sci.* 18 (10), 4934–4948. doi:10.1039/d5ee00545k
- Lou, S., Zhang, F., Fu, C., Chen, M., Ma, Y., Yin, G., et al. (2021). Interface issues and challenges in all-solid-state batteries: lithium, sodium, and beyond. *Adv. Mater.* 33 (6), 2000721. doi:10.1002/adma.202000721
- Luo, H., Du, J., Fu, J., Zhang, Q., Hu, X., Liu, B., et al. (2025). Phase-regulated ultrathin PVDF-based electrolytes for dynamic dendrite suppression in solid-state lithium metal batteries. *Nano Res.* 18 (8), 94907631. doi:10.26599/nr.2025.94907631
- Rao, Y. B., Bharathi, K. K., and Patro, L. N. (2021). Review on the synthesis and doping strategies in enhancing the Na ion conductivity of Na₃Zr₂Si₂PO₁₂ (NASICON) based solid electrolytes. *Solid State Ionics* 366–367, 115671. doi:10.1016/j.ssi.2021.115671
- Su, C., Qu, Y., Hu, N., Wang, L., Song, Z., Pei, M., et al. (2025). Rapid Na⁺ transport pathway and stable interface design enabling ultralong life solid-state sodium metal batteries. *Angew. Chem.* 64 (7), e202418959. doi:10.1002/ange.202418959
- Suh, J. H., Lee, H., Kim, J., Bae, H., Shim, J. H., Pang, W. K., et al. (2025). Strategic lithium-ion battery recycling for global resource challenges. *Carbon Neutralization* 4 (4), e70018. doi:10.1002/cnl2.70018
- Thapaliya, B. P., Wang, T., Borisevich, A. Y., Meyer, H. M., Sun, X.-G., Paranthaman, M. P., et al. (2023). *In situ* ion-exchange metathesis induced Conformal LIF surface films on cathode (NMC811) as a cathode electrolyte interphase. *Adv. Funct. Mater.* 33 (44), 2302443. doi:10.1002/adfm.202302443
- Wang, H., Sun, Y., Liu, Q., Mei, Z., Yang, L., Duan, L., et al. (2022). An asymmetric bilayer polymer-ceramic solid electrolyte for high-performance sodium metal batteries. *J. Energy Chem.* 74, 18–25. doi:10.1016/j.jechem.2022.07.010
- Wang, X., Liu, L., Hu, Z., Peng, C., Han, C., and Li, W. (2023a). High energy density aqueous zinc-chalcogen (S, Se, Te) batteries: recent progress, challenges, and perspective. *Adv. Energy Mater.* 13 (44), 2302927. doi:10.1002/aenm.202302927
- Wang, W., Yuan, W., Zhao, Z., Zhou, P., Zhang, P., Ding, M., et al. (2023b). Sandwiched composite electrolyte with excellent interfacial contact for high-performance solid-state sodium-ion batteries. *J. Colloid Interface Sci.* 652, 132–141. doi:10.1016/j.jcis.2023.08.052
- Wang, T., Zhang, M., Zhou, K., Wang, H., Shao, A., Hou, L., et al. (2023c). A hetero-layered, mechanically reinforced, ultra-lightweight composite polymer electrolyte for wide-temperature-range, solid-state sodium batteries. *Adv. Funct. Mater.* 33 (22), 2215117. doi:10.1002/adfm.202215117
- Wang, Z., Mao, Y., Sheng, L., and Sun, C. (2024). Robust solid-state Na-CO₂ battery with Na_{2.7}Zr₂Si₂PO_{11.7}F_{0.3}-PVDF-HFP composite solid electrolyte and Na₁₅Sn₄/Na anode. *ACS Appl. Mater. & Interfaces* 16 (10), 12706–12716. doi:10.1021/acsmi.4c00273
- Wang, R.-H., Zhang, Y.-Z., Wang, W., Ni, J.-H., Hu, W., Yue, L., et al. (2025a). Toward high-performance, flexible, photo-assisted all-solid-state sodium-metal batteries: screening of solid-polymer-based electrolytes coupled with photoelectrochemical storage cathodes. *Adv. Mater.* 37 (13), 2500348. doi:10.1002/adma.202500348
- Wang, S., Lu, X., Zhang, T., Kang, Y., Shi, Y., Tian, Y., et al. (2025b). Nonflammable polyfluorides-anchored quasi-solid electrolytes by chemical-crosslinking for high-safety sodium metal battery. *Adv. Funct. Mater.* (n/a), 2507147. n/a. doi:10.1002/adfm.202507147
- Wang, X., Fan, Y., Li, J., Li, X., Li, W., Wang, J., et al. (2025c). Comprehensive understanding of the Na_{1+x}Zr₂Si₆P_{3-x}O₁₂ solid-state electrolyte in advanced sodium metal batteries: a critical review. *Energy & Environ. Sci.* 18 (3), 1096–1129. doi:10.1039/D4EE04323E
- Wang, X., Li, J., Hu, Z., Li, X., Liu, L., Wang, J., et al. (2025d). Sc/Mg Co-Doping in Na₃Zr₂Si₂PO₁₂ solid-state electrolytes enables outstanding performance of sodium metal batteries. *Adv. Sci.* (n/a), e15463. doi:10.1002/advs.202515463
- Wu, C.-Y., Huang, C.-E., Luo, A.-C., Lu, W.-H., Huang, S.-C., Huang, Y.-M., et al. (2025). Enabling high-performance and high-rate-capability Na₄MnV(PO₄)₃ sodium-ion battery cathodes through tuning the NASICON framework. *J. Mater. Chem. A* 13 (4), 2716–2729. doi:10.1039/d4ta06069e
- Yang, W., Liu, Y., Sun, X., He, Z., He, P., and Zhou, H. (2024). Solvation-tailored PVDF-based solid-state electrolyte and high-voltage lithium metal batteries. *Angew. Chem. Int. Ed.* 63 (18), e202401428. doi:10.1002/anie.202401428
- Zeng, L., Bao, C., Xin, X., Lu, H., Xiong, P., Dong, X., et al. (2025). 3D NASICON ceramic skeleton enabled 18 μm-Thick high performance bicontinuous-phase ultrathin composite quasi-solid-state electrolyte. *Adv. Funct. Mater.* (n/a), e17736. n/a. doi:10.1002/adfm.202517736
- Zhang, Z., Zhang, Q., Ren, C., Luo, F., Ma, Q., Hu, Y.-S., et al. (2016). A ceramic/polymer composite solid electrolyte for sodium batteries. *J. Mater. Chem. A* 4 (41), 15823–15828. doi:10.1039/c6ta07590h
- Zheng, X., Gu, Z., Fu, J., Wang, H., Ye, X., Huang, L., et al. (2021). Knocking down the kinetic barriers towards fast-charging and low-temperature sodium metal batteries. *Energy & Environ. Sci.* 14 (9), 4936–4947. doi:10.1039/d1ee01404h
- Zheng, Q., Lu, H., Hu, Z., Liu, L., Tang, Z., Han, C., et al. (2025). Multifunctional separator design for regulating Zn²⁺ ion flux and Zn stripping in anode-less Zn metal batteries. *Nano Lett.* 25 (31), 11961–11969. doi:10.1021/acsnanolett.5c02642
- Zhou, Q., Yang, X., Xiong, X., Zhang, Q., Peng, B., Chen, Y., et al. (2022). A solid electrolyte based on electrochemical active Li₄Ti₅O₁₂ with PVDF for solid state lithium metal battery. *Adv. Energy Mater.* 12 (39), 2201991. doi:10.1002/aenm.202201991
- Zou, Z., Ma, N., Wang, A., Ran, Y., Song, T., Jiao, Y., et al. (2020). Relationships between Na⁺ distribution, concerted migration, and diffusion properties in rhombohedral NASICON. *Adv. Energy Mater.* 10 (30), 2001486. doi:10.1002/aenm.202001486